Tetragonal phases in Fe-Ga alloys: A quantitative study

A. M. Balagurov [1,2,3] I. A. Bobrikov [4] D. Yu. Chernyshov [5] A. S. Sohatsky,[1] S. V. Sumnikov [1,2] B. Yerzhanov [1,6,*] and I. S. Golovin [1,2]

[1]*Joint Institute for Nuclear Research*, Dubna, Russian Federation
[2]*National University of Science and Technology* "MISIS", Moscow, Russian Federation
[3]*Lomonosov Moscow State University*, Moscow, Russian Federation
[4]*Centre for Cooperative Research on Alternative Energies (CIC energiGUNE), Basque Research and Technology Alliance (BRTA),*
Alava Technology Park, Albert Einstein 48, Vitoria-Gasteiz 01510, Spain
[5]*SNBL at ESRF, 71 avenue des Martyrs, Grenoble, France*
[6]*Kazan (Volga Region) Federal University, 420008 Kazan, Russian Federation*

Currently, the dominant model for the formation of enhanced magnetostriction of Fe-Ga alloys is based on the assumption of the presence of microscopic inclusions with a tetragonal $L6_0$ structure in the cubic matrix of the alloy. However, no evidence for the presence of this phase in the bulk of the alloys in amounts sufficient to have a noticeable effect on the magnitude of magnetostriction has been obtained so far. To test this hypothesis, a detailed scanning of the reciprocal space of $Fe_{81}Ga_{19}Tb_{0.1}$ and $Fe_{73}Ga_{27}$ single crystals was carried out at ESRF at high photon flux stations. In particular, it was possible to reliably record superstructure diffraction peaks, the intensity of which was at a level of 2×10^{-6} from the intensity of the fundamental peaks. Nevertheless, neither the presence of superstructure diffraction peaks obviously belonging to the $L6_0$ phase nor the tetragonal splitting of the fundamental diffraction peaks into components, which could indicate the presence of this phase in the samples, was detected. Similar results were obtained using complementary methods (electron and neutron diffraction). Based on the performed analysis of the background level in the places of the expected positions of superstructure peaks of the $L6_0$ phase, it was found that the volume fraction of this phase in the $Fe_{81}Ga_{19}Tb_{0.1}$ alloy cannot exceed 0.2 %. The presence of a previously discovered X phase with hexagonal or orthorhombic symmetry in a crystal with 27 at. % Ga was confirmed.

I. INTRODUCTION

In the early 2000s, it was found that the dependence of the magnetostriction constant of $Fe_{100-x}Ga_x$ alloys on the gallium content shows two clearly defined maxima: at $x \approx 19$ and $x \approx 28$ [1–3]. At these concentrations, the magnetostriction constant $(3/2)\lambda_{100}$ of Fe-Ga single crystals at room temperature reaches ~ 400 ppm, which is roughly twenty times greater than that of pure polycrystalline iron. When alloys with Ga > 17 at. % were quenched from the $A2$ region (900 °C–1000 °C) in water, magnetostriction turned out to be 15–25 % higher than when they were slowly cooled from the same temperature, although, in general, its Ga concentration dependence was similar for both types of heat treatment. It was natural to associate a noticeable change in magnetostriction depending on the sample's prehistory (quenching, slow cooling) with the formation in the crystal of specific structural inhomogeneities with an anisotropic, possibly tetragonal, structure that violates the long-range crystalline order of the matrix with cubic symmetry. This idea was formulated in Refs. [4,5], where it was assumed that the bcc iron lattice is deformed along [100]-type directions due to the formation of short-range order

in the arrangement of Ga atoms. Calculations carried out [6] soon confirmed that pairs of Ga atoms with a tetragonal $B2$-like structure (two $B2$ cells with a common face) can play a key role in enhancing the positive magnetostriction of the Fe-Ga alloy.

In Ref. [7], it was assumed that Ga-Ga pairs can arise if, during quenching of the alloy, instead of the well-known $D0_3$ structure, a modified structure (m-$D0_3$) is formed, in which an exchange of positions has occurred between Fe and Ga atoms. The authors of Ref. [7] showed that the m-$D0_3$ structure can be described in terms of the primitive tetragonal group $P4/mmm$ and is equivalent to the $L6_0$ phase (structure prototype $CuTi_3$), which is a tetragonal distortion of the $L1_2$ phase. In addition, it was indicated in Ref. [7] that the formation of the m-$D0_3$ structure leads to the appearance in the diffraction patterns of a different set of superstructure peaks than in $D0_3$. Moreover, if the unit cell parameters in the $L6_0$ setup deviate from the $c/a = 1/\sqrt{2}$ ratio, the positions of the fundamental diffraction peaks (111, 200, etc.) split. Somewhat later, another candidate for the role of tetragonal inhomogeneities was proposed: the $D0_{22}$ phase (space group $I4/mmm$, structure prototype Al_3Ti) [8]. All these phases ($B2$, $D0_3$, $L6_0$, $D0_{22}$) at $x \approx 19$ are not at an equilibrium state in Fe-Ga alloys at room temperature, but the difference in their total energy with the energy of the disordered phase $A2$ is small and they can be formed during

*Contact author: bekarys@jinr.ru

quenching, uneven cooling, or annealing of the alloy in the $A2$ matrix and remain in it for a long time during natural or artificial aging (below 250–300 °C).

To test the ideas expressed in Refs. [4,5,7,8], experiments were performed using high-resolution transmission electron microscopy (HRTEM) [9] and diffuse neutron scattering [10], in which nanometer-scale precipitates (<2 nm) of the $D0_3$ phase and regions with short-range order (SRO), leading to tetragonal distortion of the matrix, were recorded in the $Fe_{81}Ga_{19}$ alloy. The last statement was later amended [11], but the presence of short-range-ordered Ga-Ga pairs along the basal directions of the $A2$ structure was subsequently confirmed in many experiments. For example, in Ref. [12], a detailed analysis of Bragg and diffuse x-ray scattering was carried out, measured in several directions in the reciprocal lattice of two $Fe_{82}Ga_{18}$ single crystals, one of which was quenched in water, and the second was slowly cooled. In both samples, clusters of the $D0_3$ phase (with short- and long-range order) and "$B2$ clusters", which are formed by two cells with a bcc $B2$ structure that have a common face, were found. The model calculations performed showed significant deformation of $B2$ clusters and, as a consequence, tetragonal distortion of the matrix. In principle, one can move from $B2$ clusters to domains with the $L6_0$ structure, placing them in a certain way next to each other. This topic is developed in detail in Ref. [13], where it is shown that the $Fe_{81}Ga_{19}$ alloy contains domains of local chemical order (LCO) with a tetragonal $L6_0$ structure and a diagram of their evolution ("full life cycle") during quenching and annealing in different temperature ranges is presented.

Evidence of the formation of domains with long-range order ($L > 50$ Å) and with the $D0_{22}$ structure is given in only one article [14], while information on the observation of extended ordered domains with the $L6_0$ structure has repeatedly appeared and continues to appear in the literature. Three types of experimental data can be distinguished, based on which a conclusion is made about the presence of the tetragonal $L6_0$ phase in the bulk of the alloy in the form of structurally ordered nanoinclusions: by distortion (splitting) the profiles of the fundamental diffraction peaks observed in x-ray or synchrotron diffraction experiments [15–18], on the observation of superstructure diffraction spots in selected area electron diffraction (SAED) experiments and comparison of their characteristics with model calculations [14,16,18,19], and by the presence of specific features in magnetic small-angle neutron scattering (SANS) [20–23].

These evidences were found for $Fe_{100−x}Ga_x$ in the range 17–19 at. % Ga and at $x \approx 27$, as well as in the compositions $Fe_{100−x}Ga_xRE_y$, where RE is a rare earth element. The influence of Tb on the physical and structural properties of Fe-Ga alloys has been studied in particular detail, the presence of which in an amount of ∼0.1–0.2 at. % noticeably increases the magnetostriction constant [24]. However, the reliability of these evidences is not absolute. To confirm the presence of tetragonal phases with long-range order in the bulk of the sample, it is necessary to register their inherent superstructure diffraction peaks using x-ray, synchrotron, or neutron radiation. Despite numerous attempts, not a single experiment with these radiations has yet succeeded in registering either the $L6_0$ or $D0_{22}$ phases. Individual peaks observed in some

synchrotron experiments [25,26], which were interpreted as belonging to the $L6_0$ phase, cannot be sufficient evidence for the presence of this phase in the sample. A necessary condition is the observation of several superstructure peaks. For example, in the diffraction spectra presented in Ref. [25], only one peak is observed with the same d_{hkl} as the super-structure 211 peak of the m-$D0_3$ phase (101 in the tetragonal $L6_0$ setup). Since there are no other superstructure peaks, including the strongest peak at $d \approx 4.10$ Å, in the spectra, the presence of this phase in the samples cannot be considered proven.

The interpretation of the splitting of the profiles of the fundamental diffraction peaks as a sign of the presence of the $L6_0$ phase also raises doubts, since if its tetragonal distortion is sufficiently large, two additional peaks should appear instead of one peak, as in the mentioned references. Moreover, as was shown in Ref. [27], the reason for the appearance of split diffraction peaks may be the formation of structures $A2$ and $B2$ in the near-surface layers at a depth of up to 10 μm, and which are absent in the bulk of the samples.

A specific feature of transmission electron microscopy (TEM) is the study of ultrathin samples and special methods for their preparation, which, for a number of reasons discussed below, casts doubt on the possibility of the presence of the observed effects in bulk samples. In the case of SANS, the model calculations carried out do not contradict the assumption that the observed features are associated with magnetic inclusions of the $L6_0$ phase, but, even in this case, the experimental data are not direct due to the peculiarities of the SANS method; the atomic scattering contrast between the $A2$, $D0_3$, and $L6_0$ phases is practically absent as they have a similar composition and density.

It should be noted that, in addition to inclusions $B2$ and $L6_0$, several more structural phases with a structure different from $D0_3$ were discovered in Fe-Ga alloys. In Ref. [12], and then in Ref. [28], the evidences were provided for the formation in Fe-Al and Fe-Ga alloys of a previously unobserved structural phase of type $B1$ ($a \approx 5.2$ Å, structure prototype NaCl). Another nonstandard type of ordering was discovered when studying the $Fe_{73}Ga_{27}$ single crystal with synchrotron radiation [29]. When continuously scanning a large volume of reciprocal space, many reflections (≈90% of the total number) were observed, the presence of which can be explained by assuming that they correspond to a hexagonal lattice with $a \approx \sqrt{8}a_0$, $c \approx \sqrt{12}a_0$, where $a_0 = 2.87$ Å is the lattice parameter of α-Fe. This lattice can be transformed into a primitive cubic lattice with $a \approx 6a_0$, the reflections from which coincide with all reflections belonging to the $B2$, $D0_3$, and $L6_0$ (at $c/a \approx 1/\sqrt{2}$) phases. The possible influence of these phases, which have not yet been reflected in phase diagrams, on the magnitude of magnetostriction has not yet been studied.

A number of studies have obtained estimates of the characteristic volume fractions and sizes of $L6_0$ regions in polycrystalline Fe-Ga samples: ≈5% in $Fe_{83}Ga_{17}$ (≈30 Å) [16], ≈3.6% in $Fe_{81}Ga_{19}$ (20–130 Å) [19], and ≈5% in $Fe_{83}Ga_{17}Tb_{0.1}$ (⩽100 Å) [24]. In some papers (see, for example, Refs. [14,18]), values of up to 250 Å and even up to 800 Å are indicated as the characteristic sizes of $L6_0$ precipitates. Such volumes and sizes are quite sufficient for recording

diffraction peaks of the $L6_0$ superstructure in a synchrotron experiment, despite the small value of their diffraction structural factors. Another fact that casts doubt on the reality of the formation and influence of the $L6_0$ phase on magnetostriction in bulk samples is the behavior of this physical property in the $Fe_{100-x}Al_x$ and $Fe_{100-x-y}Ga_xAl_y$ alloys. According to Ref. [30], where a comparative analysis of the magnetostriction constant of Fe-Ga and Fe-Al alloys was performed, the first maximum in the dependence of $(3/2)\lambda_{100}$ on the concentrations of Ga and Al is achieved at approximately the same values (≈ 19 at. %). In it, this value for Fe-Al alloys is $\approx 60\%$ of the Fe-Ga constant; however, no signs of the presence of the $L6_0$ phase in alloys with Al have yet been found. It is, therefore, highly likely that the peak-shaped behavior of magnetostriction in this alloy is associated with some other reasons.

The aim of this study is a comprehensive analysis of synchrotron, electron, and neutron diffraction data obtained on Fe-Ga and Fe-Ga-Tb alloys, the main purpose of which was to search for the presence of the $L6_0$ phase and any other nonstandard phases in bulk samples. We were unable to detect reliable signs of the presence of the $L6_0$ phase in any of the studied alloys. Only an upper estimate of the volume fraction of the sample that it could occupy was obtained. The only nonstandard phase, the presence of which was confirmed in the composition of $Fe_{73}Ga_{27}$, was the phase with a hexagonal or orthorhombic translational symmetry [29].

II. MATERIALS, EXPERIMENTAL TECHNIQUE, AND DATA PROCESSING

Several cast samples with nominal compositions $Fe_{81}Ga_{19}$, $(Fe_{81}Ga_{19})_{99.9}Tb_{0.1}$, and $Fe_{73}Ga_{27}$ were prepared by melting appropriate mixtures of pure components in an induction furnace under high-purity argon gas and subsequent rapid solidification in a copper mold. Their chemical compositions were confirmed with an accuracy of $\pm 0.2\%$ by energy-dispersive spectroscopy and turned out to be close to the expected, namely, $Fe_{80.5}Ga_{19.5}$, $(Fe_{81.5}Ga_{18.5})_{99.92}Tb_{0.08}$, and $Fe_{73.4}Ga_{26.6}$ (hereinafter, for brevity, the designations $Fe_{81}Ga_{19}$, $Fe_{81}Ga_{19}Tb_{0.1}$, and $Fe_{73}Ga_{27}$ are used). Their homogenization was carried out by annealing in quartz ampoules at $1000\,^\circ C$ for 1 hour, after which the samples were quenched in water.

For neutron experiments, parallelepipeds with dimensions close to $4 \times 4 \times 50\,mm^3$ were cut from the ingots. For powder synchrotron experiments, samples were crushed mechanically, followed by annealing in a capillary directly in the furnace used to study samples at high temperatures. In this case, the powders were quenched in air. In addition, for single-crystal synchrotron experiments, needlelike samples of thickness $\approx 100\,\mu m$, obtained by cutting and polishing, were etched with a mixture of ethanol-diluted HNO_3 in order to identify individual grains with a typical size of $\approx 100\,\mu m$.

To study the structure of the samples using TEM, pieces of ingots were sawn into thin plates, which were then polished to a thickness of about 0.1 mm. Disks with a diameter of 3 mm were cut from the plates. Objects for TEM were manufactured using the standard method of two-jet electrochemical polishing of disks before perforation in a 5% solution of perchloric acid in methanol, at a temperature of $-30\,^\circ C$, using a Struers Tenupol-5 installation. The object of the TEM study was a thin foil of material formed along the edge of an etched hole, about 100 nm thick.

Synchrotron diffraction experiments were performed in Grenoble on the BM01A Swiss-Norwegian Beam Lines beam line at the ESRF [31] ($\lambda = 0.6867\,\text{Å}$, sample-to-detector distance 239 mm) and the ID28 beam line of ESRF [32] ($\lambda = 0.6968\,\text{Å}$, sample-to-detector distance 244 mm). In both cases, data were recorded with hybrid pixel detectors, Pilatus 2M and Pilatus3 1M, respectively. The BM01A experiment was devoted primarily to the collection of Bragg intensities, while the ID28 data allowed a more detailed collection of diffuse scattering intensities, having a photon flux density approximately two orders of magnitude larger. The beam sizes on the samples were $0.15 \times 0.15\,mm^2$ and $0.02 \times 0.04\,mm^2$ (the values are the horizontal and vertical widths of the beam at half maximum intensity), respectively, and allowed data collection with the domination of one single crystal and only a minor contribution from the adjacent grains. The data were collected in shutterless mode with one scanning axis and an angular step per frame of 0.1°–0.25°. For such a diffraction experiment, the volume of reciprocal space covered at the end of the measurements is defined by the size and shape of the detector and the angular range covered; for a full sphere of rotation, the covered volume is a torus. The reciprocal volume covered at the BM01A experiment is a torus centered at node 000; the ID28 data cover a smaller reciprocal volume displaced away from 000. At variance with the BM01 bending magnet beamline, which focuses on the Bragg data, the ID28 source provides better statistics for weak intensities, but strong Bragg reflections of the parent phase are frequently overexposed. For both diffractometers, the instrumental resolution is similarly defined by the sample and beam size, the sample-to-detector distance, the detector pixel size, and the divergency of the incoming and scattered beams; the parameters were set so that the instrumental broadening of the diffraction features was less than the detector pixel. Experimental data were treated using standard software, including SNBL ToolBox, CrysAlis, and ID28 tools under development.

TEM studies were performed on a Talos F200i (S)TEM electron microscope (Thermo Fisher Scientific) with field emission electrons, operating at an accelerating voltage of 200 kV. The studies included obtaining images of the microstructure of samples in bright- and dark-field modes and recording electron diffraction patterns from the region of a single grain.

Neutron diffraction patterns were measured using a high-resolution Fourier diffractometer (HRFD) at the IBR-2 pulsed reactor at JINR (Dubna) [33]. The HRFD is a time-of-flight diffractometer with a fast Fourier chopper and the ability to switch between high-resolution ($\Delta d/d \approx 0.0015$) and high-intensity, medium-resolution ($\Delta d/d \approx 0.015$) modes. The high-resolution neutron diffraction patterns were then used to analyze the diffraction peak profiles. In the second mode, the intensity of the spectrum increases by approximately ten times and it was used to record weak superstructure peaks. A more detailed description of the method is contained in the review article of Ref. [34], which also provides crystallographic data

for the structural phases $A1$, $A2$, $B2$, $D0_3$, and $L1_2$ found in Fe-Ga alloys.

III. RESULTS

A. Identification of the $D0_3$ and $L6_0$ ordered phases

The atomic structure of the $D0_3$ phase of Fe-Ga alloys is given in Ref. [35] and has been repeatedly described in the literature (see, for example, Refs. [7,8]). This phase corresponds to a cubic space group $Fm\bar{3}m$ with a unit cell parameter $a \approx 5.81$ Å, $Z = 4$ (Fe$_{75}$Ga$_{25}$, 20 °C). The standard space group for the $L6_0$ phase is $P4/mmm$ with $a \approx a(D0_3)/\sqrt{2} \approx 4.11$ Å and $c \approx a(D0_3)/2 \approx 2.91$ Å, $Z = 1$. In $L6_0$, with a completely ordered stoichiometric composition of Fe$_3$Ga, Ga atoms occupy the (1a) (0, 0, 0) position, Fe atoms are at the centers of the faces (1/2, 1/2, 0), etc. It is often convenient to discuss the properties of this phase as an m-$D0_3$ structure, i.e., within the same unit cell as $D0_3$, but with an alternative ordering scheme based on Ga-Ga pairs along [100]-type directions [7]. Below, depending on the context, both designations (m-$D0_3$ and $L6_0$) will be used.

In Ref. [14], it was shown that the total energy of the $L6_0$ phase is related to its tetragonality, and a comparison was made with the energies of the $D0_3$ and $L1_2$ phases. With complete coherence of the unit cells of the $D0_3$ and $L6_0$ phases, the degree of tetragonality is $c/a = 1/\sqrt{2} = 0.707$. As the c/a ratio increases, the total energy smoothly decreases and at $c/a > 0.780$ the $L6_0$ phase becomes energetically more favorable than $D0_3$, and a further increase to $c/a = 1$ corresponds to the $L6_0 \rightarrow L1_2$ transition. It is obvious that any deviation of c/a from $1/\sqrt{2}$ should lead to splitting of some of both the superstructure and fundamental diffraction peaks (Fig. S1 in the Supplemental Material [36]). The unit cell parameters of the $L6_0$ phase and, accordingly, the degree of tetragonality given in the literature differ noticeably from each other; for example, $a = 4.05$ Å, $c = 2.87$ Å, $c/a = 0.709$ [13] or $a = 4.10$ Å, $c = 2.98$ Å, $c/a = 0.727$ [14]. If $c/a \geqslant 0.719$, the peak splitting would be easily observed in the diffraction patterns published in Refs. [15–18], despite the broadening of the peaks due to the size effect. But, none of the listed studies observed splitting of peaks attributed to the $L6_0$ phase.

Fully ordered $D0_3$ and $L6_0$ phases are only possible for the stoichiometric composition Fe$_3$Ga = Fe$_{12}$Ga$_4$ = Fe$_{75}$Ga$_{25}$ with four formula units in the $D0_3$ unit cell and one formula unit in $L6_0$. In the diffraction pattern of such a composition, two groups of Bragg peaks can be distinguished, which are usually called fundamental (their intensity does not depend on the degree of ordering of Fe and Ga atoms) and superstructure. For the $D0_3$ phase, the fundamental peaks satisfy the condition $h + k + l = 4n$ (220, 400, etc.). For $L6_0$, the fundamental peaks are those allowed in space group $Fm\bar{3}m$ (111, 200, etc.). For superstructure peaks, it is convenient to compare the extinction rules for the $D0_3$ and m-$D0_3$ unit cells. In $D0_3$, peaks with all odd or even Miller indices are allowed (111, 200, etc.). If in m-$D0_3$ Ga-Ga pairs are aligned along the [001] direction, then the Miller indices of superstructure peaks must satisfy the conditions $h + k = 2n$, $l = 2n$ (110, 200, 002, etc., in cubic notation).

The structural factors, normalized to the number of formula units, of both the fundamental (F_F) and superstructure (F_S)
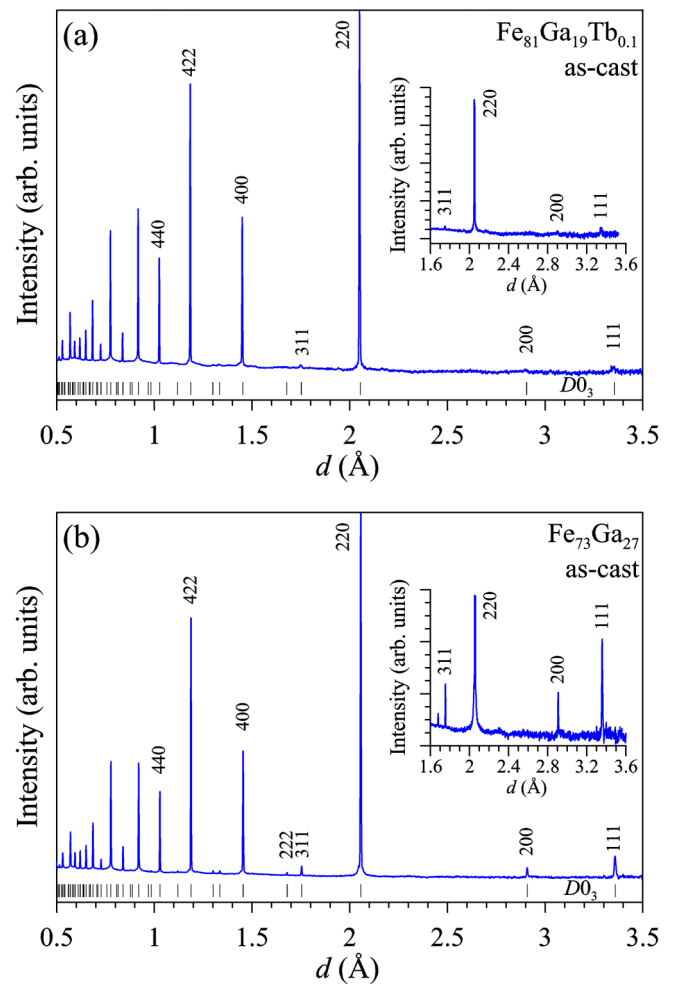
FIG. 1. High-resolution neutron diffraction patterns of (a) Fe$_{81}$Ga$_{19}$Tb$_{0.1}$ and (b) Fe$_{73}$Ga$_{27}$ in the as-cast state, measured at room temperature. Vertical ticks indicate calculated peak positions. The Miller indices of several first peaks of the $D0_3$ phase are specified. In the insets, the scale along the ordinate axis is increased.

peaks are the same for both $D0_3$ and $L6_0$ phases and are given by the expressions

$$F_F = 3b_{Fe} + b_{Ga}, \quad F_S = b_{Fe} - b_{Ga}, \tag{1}$$

where b_{Fe} and b_{Ga} are the atomic scattering factors in the case of x-ray or synchrotron radiation or the coherent scattering lengths in the case of neutron diffraction. Equations (1) assume that the composition is stoichiometric (Fe$_{75}$Ga$_{25}$) and all the atoms occupy high-symmetry positions. It is the magnitude of the structural factors that determines the difference in the intensities of the two types of diffraction peaks. For compositions with impaired stoichiometry, for example, for Fe$_{81}$Ga$_{19} \approx$ Fe$_{3.25}$Ga$_{0.75}$ = Fe$_{13}$Ga$_3$, the extinction rules mentioned above may be violated. For example, if an excess Fe atom replaces Ga only in a certain position, peaks forbidden for the stoichiometric composition will appear in the diffraction pattern.

For illustration, neutron diffraction patterns of two studied compositions (Fe$_{81}$Ga$_{19}$Tb$_{0.1}$ and Fe$_{73}$Ga$_{27}$), measured with resolution $\Delta d/d \approx 0.002$, are shown in Fig. 1. It can be seen

that the intensity ratios of the fundamental peaks in both compositions are approximately the same, while the superstructure peaks of the $D0_3$ phase are noticeably more intense in the sample with 27 at. % Ga, which is due to the large volume of this phase. There are no signs of the $L6_0$ superstructure peaks in these patterns. The absence of the $L6_0$ phase also follows from the analysis of the fundamental peaks, in which there are no signs of splitting, and their widths are only slightly greater than the widths of the peaks of standard powders (Al_2O_3, $La^{11}B_6$) (Fig. S2 in the Supplemental Material [36]), which is due to some level of microstrain in the cast samples.

To quantify the fraction of structurally ordered domains in the sample volume based on powder diffraction data, it should be taken into account that in the absence of texture effects, the intensities of superstructure (I_S) and fundamental (I_F) peaks are

$$I_S \sim V_S \xi^2 j_{hkl} L_{hkl} |F_S|^2 \exp(-W_{hkl}),$$
$$I_F \sim V_F j_{hkl} L_{hkl} |F_F|^2 \exp(-W_{hkl}) y_{hkl}, \qquad (2)$$

where V_S is the fraction of the sample volume occupied by the ordered phase, V_F is the volume in which fundamental peaks are formed, $\xi(T)$ is the temperature-dependent degree of atomic ordering, $0 \leqslant \xi(T) \leqslant 1$, j_{hkl} is the multiplicity, L_{hkl} is the Lorentz factor, (hkl) is a particular set of Miller indices, F_S and F_F are structural factors, $\exp(-W_{hkl})$ is the Debye-Waller factor, and y_{hkl} is the extinction correction for the intensities of the fundamental diffraction peaks. Due to the smallness of the structure factors of superstructure peaks, the correction for extinction is not significant for them.

In the case of neutron diffraction, the calculation of structure factors of peaks should be performed with the values $b_{Fe} = 9.45$ and $b_{Ga} = 7.29$ fm (1 fm $= 10^{-13}$ cm); in the case of photons, to estimate the value of the structure factors of peaks with large d_{hkl}, instead of b, the atomic numbers of elements can be used: $Z_{Fe} = 26$, $Z_{Ga} = 31$. For the values for the ratio of structure factors of the superstructure and fundamental peaks, we obtain $F_S/F_F = 0.061$ for neutrons and 0.046 for photons. The Debye-Waller factor appearing in Eqs. (2) can be represented as $DW = \exp[-B/(2d_{hkl})^2]$, where B is a temperature-dependent measure of smearing of atoms near ideal positions, which for Fe-based alloys at room temperature (RT) is about 0.5 Å^2. At $d_{hkl} > 1.5$ Å, the correction for this factor does not exceed 10% and, to a first approximation, it can be neglected.

A special issue is the setting of the V_F value, which represents the volume of the sample in which the fundamental peaks are formed. When the tetragonal lattice distortion of the $L6_0$ phase is close to $c/a = 1/\sqrt{2}$ and the crystal lattices of ordered clusters and the matrix are completely coherent, the fundamental diffraction peaks are formed throughout the entire volume of the sample. If the splitting of the peaks of the $L6_0$ phase is large, then it is possible to determine the intensity of the fundamental peaks associated only with scattering from the matrix, and V_F is equal to the sample volume minus the volume of the clusters. If the volume occupied by the clusters is not large, then the real difference in the values of V_F determined in these two cases is also not large.

To estimate the intensities of the neutron superstructure peaks of both $D0_3$ and $L6_0$ phases, it is necessary to compare the intensities of the reflection orders, which makes it possible to avoid texture corrections. For example, for neutron peaks 200 and 400 we have $I_{200}/I_{400} = (Q_S/V_F) \times 2^4 \times 0.061^2 = 0.06(Q_S/V_F)$, where the $Q_S = V_S \xi^2$ factor is introduced, and the value 2^4 is the ratio of the Lorentz factors, which for a time-of-flight diffractometer are defined as $L_{hkl} \sim d_{hkl}^4$. Further assuming $\xi = 1$ and $V_S/V_F = 1/3$ (clusters of the $D0_3$ phase are completely ordered and occupy 1/3 of the sample volume), we obtain that the intensity of superstructure peak 200 of the $D0_3$ phase is about 0.02 of the intensity of fundamental peak 400. An illustration of the superstructure peaks of both phases in the large-d_{hkl} range for the Fe_3Ga alloy is given in Fig. S3 of the Supplemental Material [36]. The $L6_0$ pattern is calculated for a $c/a = 0.72$ tetragonal distortion, which leads to a clearly visible splitting of some peaks.

To correctly determine the Q_S factor in the case of neutron diffraction, it is necessary to take into account that the intensity of the superstructure peaks measured at room temperature can be noticeably increased due to the magnetic contribution ($T_C \approx 690\,°C$ for 19 at. % Ga). A model calculation for a ferromagnetic structure (FullProf package) with $\mu_{Fe} = 2.2\mu_B$ showed that for several first peaks, the magnetic contribution at RT is approximately three times higher than the nuclear contribution ($I_{mag}/I_{nuc} = 3.2$ for 111, $I_{mag}/I_{nuc} = 2.8$ for 200).

From the above estimates it follows that the problem of detecting superstructure peaks of the $D0_3$ and $L6_0$ phases is difficult, but completely solvable. For example, in the $Fe_{81}Ga_{19}$ alloy $D0_3$ clusters appear after annealing at high temperatures ($\approx 900\,°C$, 30 min) and slow cooling to room temperature [37,38]. Their volume fraction does not exceed 15%, and the degree of ordering is about 80%, and, nevertheless, superstructure peaks of this phase are reliably observed in x-ray [37], synchrotron [29], and neutron diffraction experiments [38]. A similar situation should be observed with respect to the $L6_0$ phase. In Refs. [15,18], the splitting of the fundamental peak 200 of the $A2$ phase at elevated temperatures is interpreted as the appearance of the $L6_0$ phase in an amount comparable to and even exceeding the proportion of the $A2$ phase; however, there are no superstructure peaks in the measured spectra.

B. TEM data

Using this technique, SAED diffraction patterns were obtained for the $Fe_{81}Ga_{19}$ and $Fe_{73}Ga_{27}$ alloys. In the first sample, no other phases except $A2$ and $D0_3$ could be detected (Fig. 2). The superstructure reflections of the $D0_3$ phase in this sample are noticeably broadened (diffuse) and have low intensity, which is consistent with the model of $D0_3$ clusters dispersedly distributed in the $A2$ matrix. However, no spatial separation of these phases was detected in the TEM images.

Analysis of diffraction patterns of the $Fe_{73}Ga_{27}$ sample with different orientations of its grains revealed the presence of the $D0_3$ phase, which is the main phase, or matrix, and another unknown phase X, which is also built on the basis of the bcc lattice ($A2$), but differs from $D0_3$ in a less symmetrical ordering motif of Fe and Ga atoms. In the image of one of the main zones of the matrix (Fig. 3; the other zone is shown in Fig. S4 of the Supplemental Material [36]), the diffraction patterns of phase X are presented in the form of
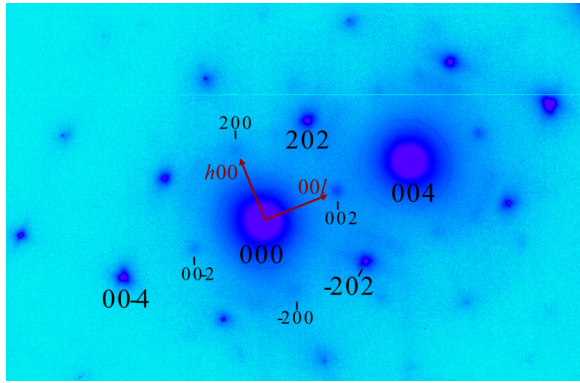
FIG. 2. TEM diffraction pattern of the $Fe_{81}Ga_{19}$ sample, $h0l$ reciprocal space layer. Directions $[h00]$ and $[00l]$ are indicated. Only reflections corresponding to phases $A2$ and $D0_3$ are observed. The diffraction conditions of the survey were chosen in such a way that the intensity of some of the superstructure reflections of the $D0_3$ phase was maximum.

two or three superimposed zones of superstructure reflections corresponding to different orientations of the same reciprocal superlattice.

All visible superstructure units of the X phase form a hexagonal crystalline system, oriented with axis 6 along one of the four directions [111] of the bcc lattice. In this case, the nodes of the hexagonal reciprocal lattice X include the nodes of the reciprocal lattice of the bcc crystal with the orientation relationship

$$001_h(=c_h^*) = 222_{bcc}/12, \quad 100_h(=a_h^*, b_h^*) = 112_{bcc}/6, \quad (3)$$

where the indices h and bcc indicate that the nodes belong to the hexagonal crystal system or to the reciprocal lattice of the bcc crystal, respectively. However, it is possible that the structure of the ordered X phase is neither hexagonal nor trigonal. This is indicated by a less symmetrical system of reflection
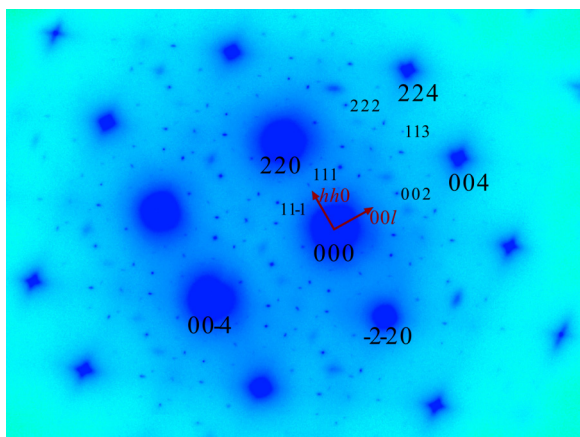
FIG. 3. TEM diffraction pattern of the $Fe_{73}Ga_{27}$ sample, hhl reciprocal space layer. Directions $[hh0]$ and $[00l]$ and the Miller indices of several fundamental (220, 004, 224, etc.) and superstructure (111, 002, 113, etc.) peaks of the $D0_3$ phase are indicated. Most reflections are related to the X phase, the lattice of which is hexagonal or orthorhombic. Formally, all visible reflections of this phase can be attributed to a cubic lattice with $a = 3a(D0_3) \approx 17.34$ Å.

extinctions in the X reciprocal lattice, the analysis of which allows us to attribute it to a lower-symmetric Laue class, probably to the orthorhombic *mmm*. It follows that crystallites (twins) of phase X can occupy 12 possible nonequivalent orientation positions in the lattice of a bcc crystal.

Bright-field TEM images (Figs. S5(a) and S5(b) of the Supplemental Material [36]) show many inclusions of another phase, both individual and combined into clusters, in the grains of the $Fe_{73}Ga_{27}$ sample. This is not a surface effect that is evidenced by their density in the image, which increases with the thickness of the foil. The inclusions are built coherently into the $D0_3$ matrix. This is evidenced by elastic stresses in the matrix around the inclusions, clearly visible in the dark-field image with precise Bragg orientation (Fig. S5(b) of the Supplemental Material [36]). Dark-field TEM images of the superstructure reflection (024) of phase X (Figs. S5(c) and S5(d) of the Supplemental Material [36]) show that it is this phase that forms the observed coherent inclusions in the $D0_3$ matrix. The dark-field images also show that the X inclusions are extended and oriented in the ⟨111⟩ directions. Many inclusions are divided into twins with stacking faults along the $\{111\}_h$ and $\{011\}_h$ planes at the boundaries between them.

The described phase X cannot be considered a candidate for the role of the tetragonal phase $L6_0$, as it follows from symmetry considerations. However, it should be noted that in complex diffraction patterns obtained from a set of X crystallites embedded in a bcc lattice in different orientations, some sample from the sum of X reflections can depict the complete $L6_0$ reciprocal lattice. It is possible that this circumstance may be the reason for erroneous interpretation of the results of diffraction experiments in TEM, especially in connection with the extremely low intensity of superstructure diffraction from ordered Fe-Ga alloys.

C. Synchrotron data

This section presents data obtained for the $Fe_{81}Ga_{19}Tb_{0.1}$ and $Fe_{73}Ga_{27}$ alloys at the BM01A and ID28 stations. For $Fe_{81}Ga_{19}Tb_{0.1}$, measurements of the intensity distribution in the reciprocal space were carried out at $T = 20\,°C$ at station BM01A and at elevated temperatures (20 °C, 350 °C, 450 °C, and 680 °C) at ID28. The $Fe_{73}Ga_{27}$ alloy was measured on ID28 at room temperature.

From the $Fe_{81}Ga_{19}Tb_{0.1}$ powder diffraction pattern measured on BM01A, it follows that in the initial state the sample is in the disordered $A2$ phase (Fig. S6 of the Supplemental Material [36]) with a small presence ($\approx 0.2\%$) of the $A1$ phase (disordered state of the $L1_2$ phase). But there are no signs of superstructure peaks of the $D0_3$ and $L6_0$ phases. Measurements of the same sample at station ID28, the photon flux at which is ~100 times higher than at BM01A, showed [Fig. 4(a)] that, in fact, already in the initial state of the sample there are signs of ordering, as evidenced by the presence of weak diffuse superstructure $D0_3$ spots. Rapid heating to 350 °C led to the formation of narrow, clearly visible [Figs. 4(b)–4(d)] superstructure peaks of this phase. Three different cross sections of the reciprocal space of a single crystal are shown in Fig. 4, but in none of them can any signs of superstructure reflections of the $L6_0$ phase be de-
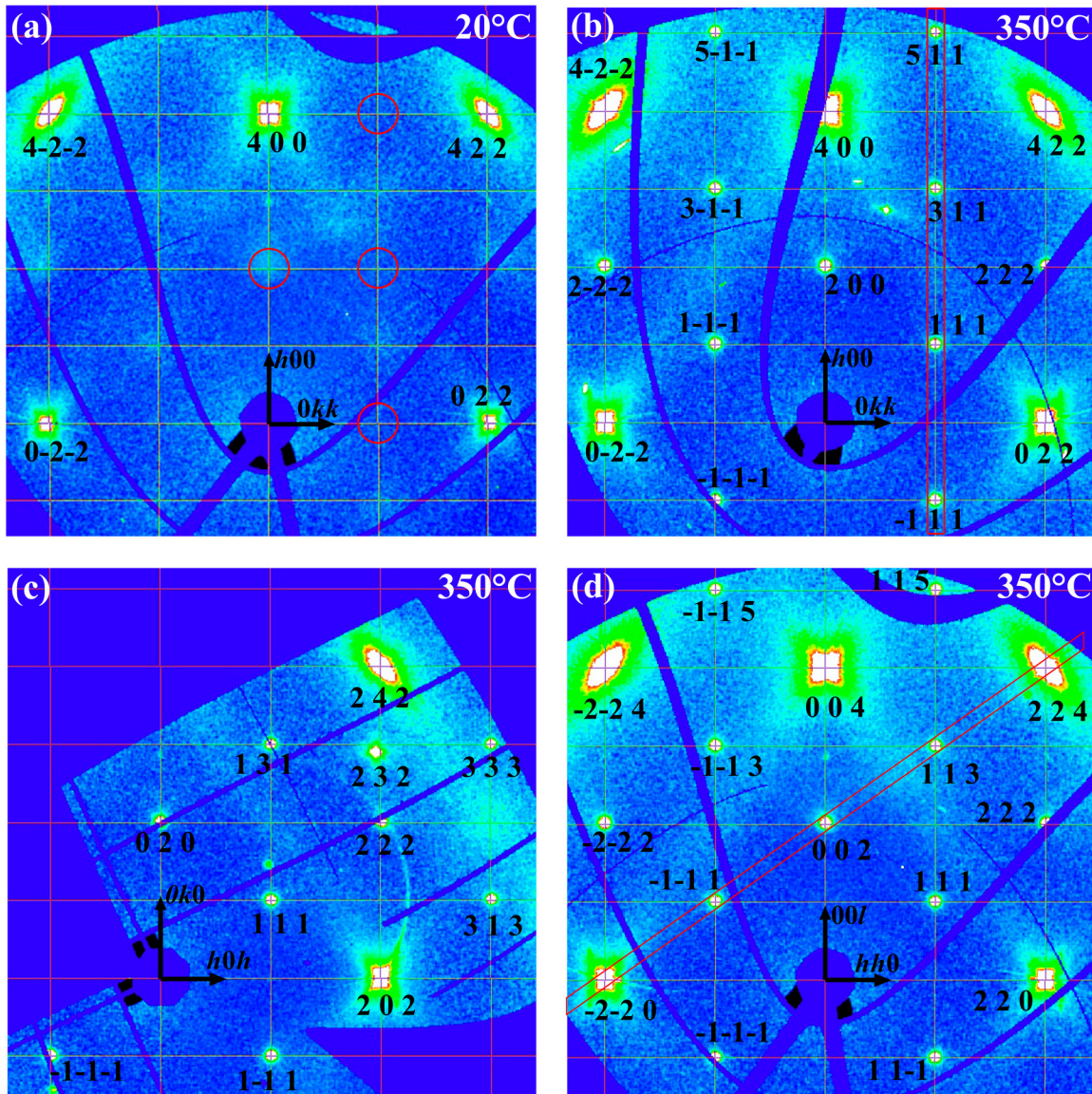
FIG. 4. Two-dimensional (2D) cross sections of the reciprocal space of the $Fe_{81}Ga_{19}Tb_{0.1}$ alloy, measured at (a) 20 °C (hkk layer) and [(b)–(d)] 350 °C at ID28. For $T = 350$ °C, three layers are shown: (b) hkk, (c) hkh, and (d) hhl. Grids and Miller indices of reflections are given for the $D0_3$ cell with parameter $a \approx 5.78$ Å. The Miller indices of strong (fundamental) reflections satisfy the condition $h + k + l = 4n$. Circles in (a) indicate places of possible appearance of superstructure reflections of the $L6_0$ phase. One-dimensional (1D) visualizations of the intensity distributions in the highlighted directions [$h\ h\ h + 2$] and [$h11$] are shown in Figs. 5 and 6.

tected. The intensity distributions measured at 350 °C along two directions in reciprocal space are shown in Figs. 5 and 6. It can be seen that the intensities of the superstructure peaks are ~500 times lower, and their width is noticeably (about two times) larger than the corresponding characteristics of the fundamental peaks of the $D0_3$ phase. The temperature (up to 450 °C) evolution of diffraction patterns is shown in Fig. S7 of the Supplemental Material [36]. When moving from 350 °C to 450 °C and holding for 1 hour, the intensity and width of the peaks decrease by almost threefold. With further heating to 680 °C, the structure passed into a disordered state.

For standard Poisson statistics, background fluctuations with an average value of I_b are $\Delta I_b = \pm D_b^{1/2} = 2I_b^{1/2}$, where D_b is the variance of the count distribution. From a simple analysis it follows that a diffraction peak can be observed if its amplitude satisfies the condition $A_p > 2\Delta I_b$. This condition can be used to estimate the upper limit of the peak amplitude. Assuming that the profiles of the superstructure peaks of the $D0_3$ and $L6_0$ phases are approximately the same, we can estimate their intensity from the amplitude of the peaks and then use formulas (1) to obtain the upper limit of the $Q_S = V_S\xi^2$ factor. The intensity distribution along one of the directions in reciprocal space, where superstructure peaks of the $L6_0$ phase could appear, is shown in Fig. 6.

It can be seen that at the site of their possible appearance there is really nothing but background fluctuations. Using the known background level and experimental values of the
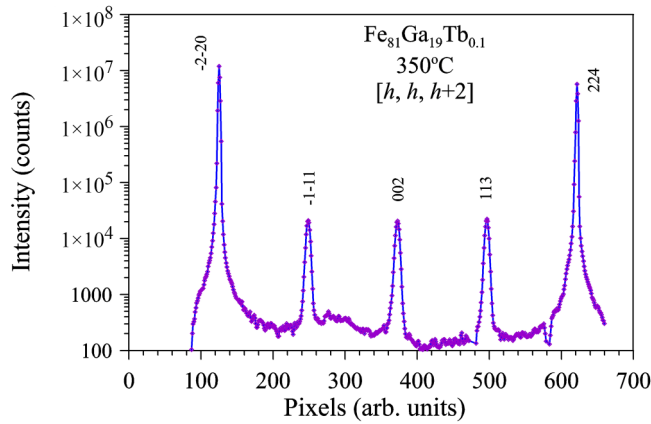
FIG. 5. 1D scan in the $[h\ h\ h+2]$ direction in the *hhl* layer (Fig. 4) of the $Fe_{81}Ga_{19}Tb_{0.1}$ alloy at 350 °C, ID28 station. The fundamental peaks (-2–20 and 224), which are heavily overexposed, and superstructure peaks of the $D0_3$ phase are visible. The ordinate scale is logarithmic.

intensities of superstructure peaks of the $D0_3$ phase at $T = 350$ °C, it was found that for the $Fe_{81}Ga_{19}Tb_{0.1}$ alloy the $Q_S = V_S\xi^2$ factor for $L6_0$ does not exceed 0.016 in comparison with the same factor for $D0_3$, i.e., $Q_S(L6_0) \leqslant 0.004$ $Q_S(D0_3)$. The estimate of Q_S for the $D0_3$ phase, obtained from the neutron data (see next section), led to a value of $Q_S \approx 0.13$. Accordingly, assuming the same degree of atomic ordering of both $D0_3$ and $L6_0$ structures, for $L6_0$ we find that its fraction does not exceed 0.0005 of the sample volume. This estimate of the volume fraction of the $L6_0$ phase should be considered minimal; under other assumptions about the degree of ordering and the fraction of the $D0_3$ phase, it may increase slightly, but not exceed the value $V_S(L6_0) \approx 0.002$.

One of the sections of the reciprocal space of a $Fe_{73}Ga_{27}$ single crystal is shown in Fig. 7. It is clear that, in addition to the reflections of the cubic $D0_3$ phase with $a \approx 5.78$ Å, there are many reflections that do not belong to the crystal lattice of
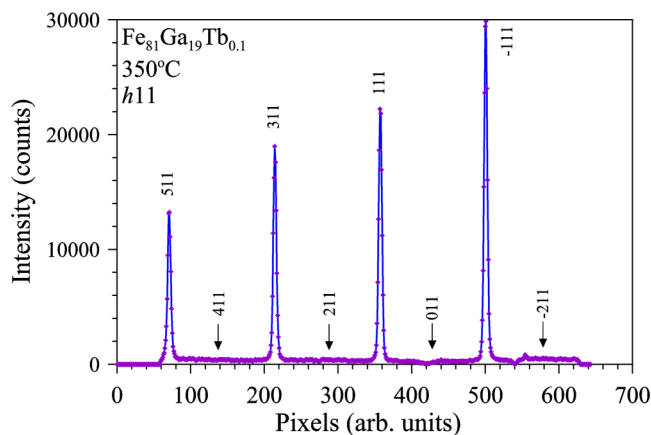
FIG. 6. 1D scan in the $[h11]$ direction in the *hkk* layer (Fig. 4) of the $Fe_{81}Ga_{19}Tb_{0.1}$ alloy at 350 °C, ID28 station. Only superstructure diffraction peaks of the $D0_3$ phase are visible. The locations where superstructure peaks of the $L6_0$ phase could appear are indicated by arrows. The peak indices of this phase are given in the m-$D0_3$ setup.
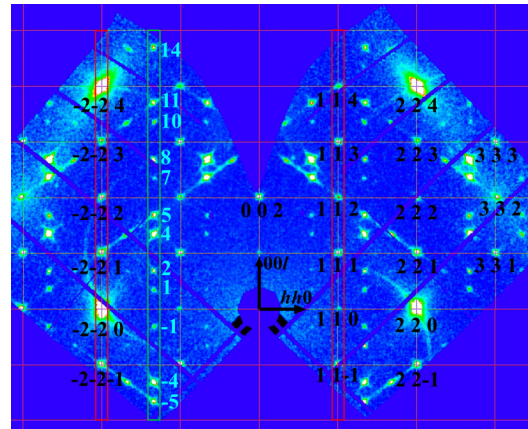
FIG. 7. *hhl* reciprocal space layer reconstructed from diffraction data; the $Fe_{73}Ga_{27}$ alloy at 20 °C, ID28 station. Grids and Miller indices of reflections are given for the $D0_3$ cubic cell with $a \approx 5.78$ Å. The Miller indices of strong (fundamental) reflections satisfy the condition $h + k + l = 4n$. The Miller indices of superstructure reflections, which are allowed in the $D0_3$ or m-$D0_3$ phases, are indicated. The remaining observed reflections belong to the cubic lattice with a parameter tripled relative to the $D0_3$ cell. In the highlighted direction $[4/3\ 4/3\ l]$ their l indices are indicated. 1D visualizations of the intensity distributions in the highlighted directions are shown in Fig. 9.

this phase. This fact was first established in Ref. [29], where it was shown that all observed reflections can be indicated in a cubic lattice with $a = 3a(D0_3) \approx 17.34$ Å, or more correctly in a hexagonal lattice with $a \approx \sqrt{2}a(D0_3)$, $c \approx \sqrt{3}\ a(D0_3)$ (Fig. 8), in which the indexing can be performed for 100% of the observed Bragg spots. Obviously, it is the same particular phase, which is observed in the TEM photographs (phase *X*) shown in Fig. 3.
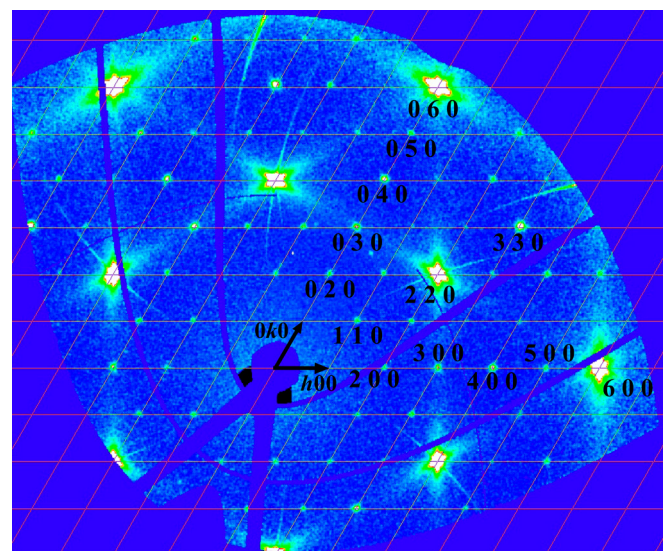
FIG. 8. 2D layer of the reciprocal space of the $Fe_{73}Ga_{27}$ alloy at 20 °C, ID28 station. The grid corresponds to a hexagonal lattice with parameters $a = 8.291$ Å, $c = 10.143$ Å, and cross section $hk0$. This grating corresponds to 100% of the visible diffraction reflections.
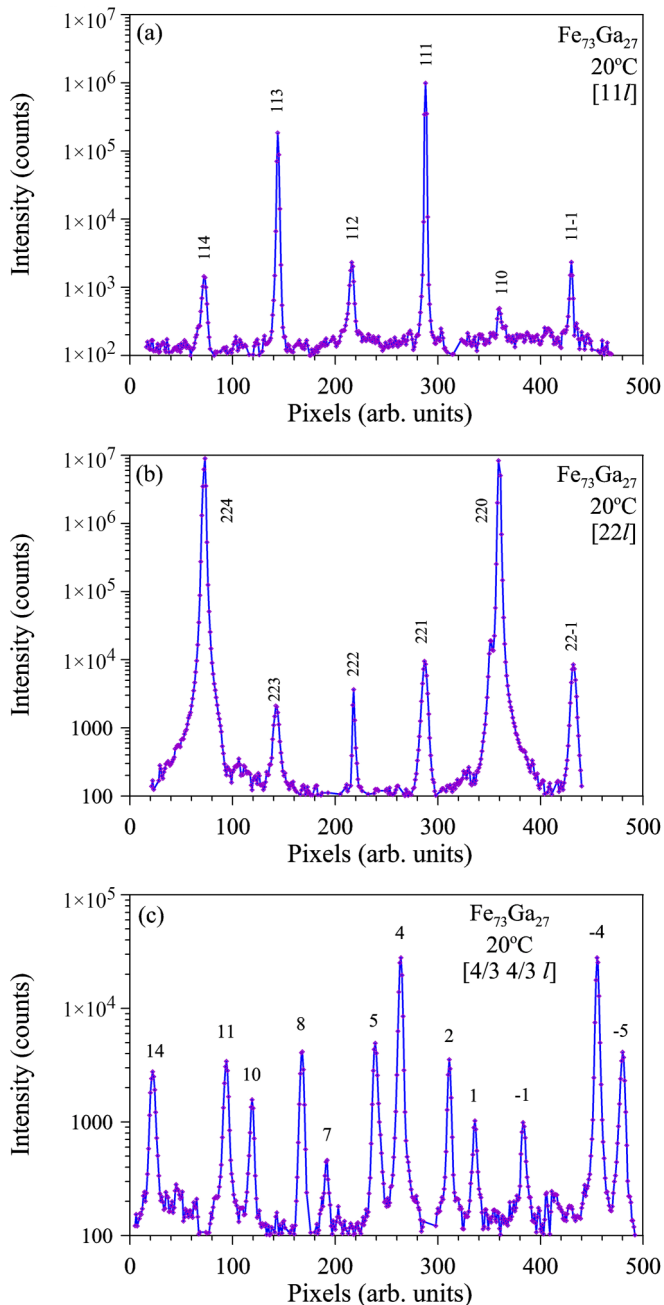
FIG. 9. 1D scans in the directions [1 1 l], [2 2 l], and [4/3 4/3 l] in the *hhl* layer (Fig. 7) of the $Fe_{73}Ga_{27}$ alloy at 20 °C, ID28 station. In (a) and (b) the Miller indices are given for a primitive cubic cell with $a \approx 5.78$ Å; in (c) the l indices (tripled) are the same as in Fig. 7. The ordinate scale is logarithmic. The fundamental peaks 224 and 220 in (b) are heavily overexposed.

The measured distributions of scattering intensity in three directions in the {*hhl*} cross section are shown in Fig. 9. In addition to the fundamental peaks (224 and 220), intense superstructure peaks of the $D0_3$ phase (113 and 111) and weaker peaks (114, 112, and 110) are clearly visible. These last peaks could be attributed to $L6_0$, but in reality they are part of Bragg reflections that belong to the phase with a hexagonal lattice.

In the intensity distribution along the [4/3 4/3 l] direction [Fig. 9(c)], none of the visible peaks belongs to $D0_3$ or

$L6_0$, and their positions in the reciprocal lattice correspond to the period $3a(D0_3)$, as follows from the graph shown in Fig. S8 of the Supplemental Material [36]. The intensities of the peaks of this phase *X* with yet unknown structure are at the level of 1/1000 of the intensity of the superstructure peaks of the $D0_3$ phase, which, in turn, are ~500 times weaker than the fundamental peaks. From these estimates it follows that for Fe-Ga alloys at the ID28 station it is possible to reliably register diffraction peaks not exceeding the level of 2×10^{-6} from the intensity of the A2 phase peaks. The peaks of the *X* phase are 2–2.5 wider than the fundamental and superstructure peaks of the $D0_3$ phase, which indicates the smaller sizes of the coherent scattering regions responsible for the formation of this phase.

D. Neutron data on the phase composition and microstructure of alloys

The main factors determining the effectiveness of neutron diffraction studies of Fe-Ga-type alloys are their large penetration depth and large beam cross section, which make it possible to obtain proper volume-averaged data on the structure of the material, not distorted by surface effects or structural inhomogeneity. In addition, it should be noted that the relatively high contrast of neutron scattering on Fe and Ga leads to increased, with respect to x rays, intensity of superstructure peaks linked to the ordering. The results of our previous neutron diffraction studies of Fe-Ga alloys are reported in Refs. [38–41] for the $Fe_{81}Ga_{19}Tb_{0.1}$ and $Fe_{73}Ga_{27}$ compositions, respectively. They were obtained on samples prepared using various options and in different final states: after rapid cooling of a small ingot in a copper mold, after slow cooling of a relatively massive ingot in a graphite mold, and after heating and subsequent controlled cooling.

From the full set of the data obtained, it follows that when the $Fe_{81}Ga_{19}$ alloy is doped with terbium in an amount of 0.1–0.3 at. % in the as-cast state (in a copper mold), its microstructural organization is a disordered matrix A2, in which some number of clusters with a $D0_3$ ordered structure are dispersedly distributed with characteristic sizes from 100 to 300 Å. The formulas given in Sec. III A allow the ratio $(V_S \xi^2)/V_F$ to be estimated from the measured I_S/I_F ratios since all other factors are known. To eliminate the influence of texture, the intensities of the reflection orders, for instance, I_{200} and I_{400}, were used for calculations. An estimate of the extinction coefficient for the fundamental peaks ($y_{hkl} \approx 0.8$ for 400 peak) was obtained from a comparison of the intensities of several orders of reflection (220/440, 400/800, and 422/844). As a result, for the $Fe_{81}Ga_{19}Tb_{0.1}$ composition, then measured at ID28, it was found that $(V_S \xi^2)/V_F = 0.14 \pm 0.02$. Since direct separate determination of the values of V_S and ξ from diffraction data is impossible, in order to determine the fraction of the sample volume occupied by clusters of the $D0_3$ phase and the degree of ordering of their structure, one must be guided by indirect data. The characteristic sizes of coherently scattering domains, L_{coh}, corresponding to clusters can be judged from the dependence of the widths of superstructure peaks on temperature when the sample is heated or cooled. The corresponding dependencies are shown in Fig. 10.
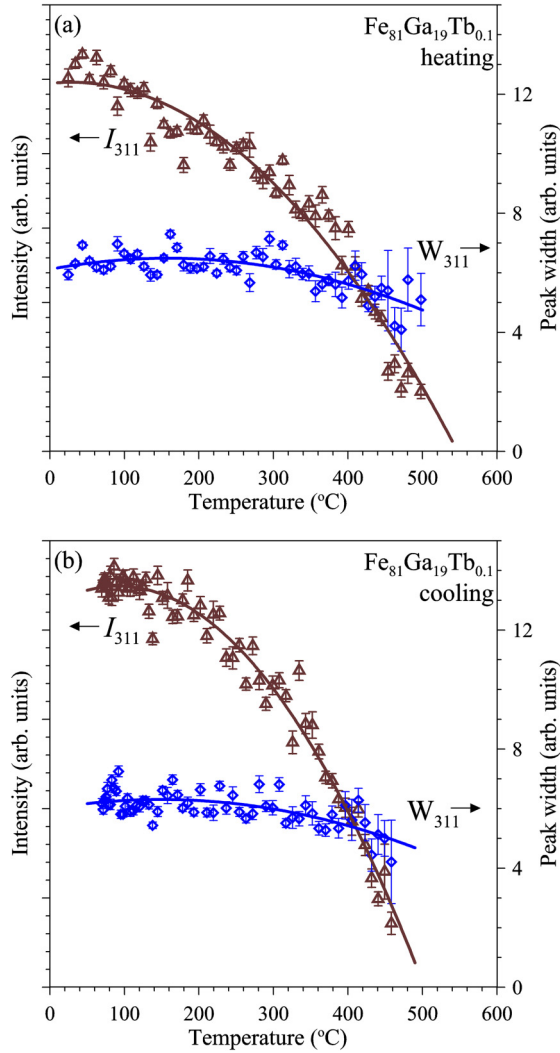
FIG. 10. Intensity (left scale) and width (right scale) of neutron diffraction superstructure peak 311 of the $Fe_{81}Ga_{19}Tb_{0.1}$ alloy as a function of temperature during (a) heating and (b) cooling.

FIG. 11. Medium-resolution neutron diffraction pattern of the $Fe_{81}Ga_{19}Tb_{0.1}$ alloy for large d_{hkl} spacings. There are fundamental and superstructure peaks of the $D0_3$ phase and weak peaks of the $A1$ phase. The locations where superstructure peaks of the $L6_0$ phase could appear are indicated by arrows. The peak indices of this phase are given in the m-$D0_3$ setup.

It follows from them that there are no significant changes in the width of peak 311 either during heating or cooling. From the excess of the peak width over the contribution of the resolution function, an estimate of the characteristic cluster size was obtained as $L_{coh} \approx 300$ Å, which varies only slightly with temperature. This fact indicates that changes in the intensities of superstructure peaks, also shown in Fig. 10, are mainly determined not by the volume fraction occupied by clusters of the $D0_3$ phase but by the degree of ordering of their structure. At $T < 100\,°C$, the intensities of superstructure peaks reach a plateau, which can be interpreted as an approach to complete ordering of the structure. This means that $\xi \approx 1$ and, in addition, assuming $V_F \approx 1$, we obtain that in the $Fe_{81}Ga_{19}Tb_{0.1}$ alloy $V_S = 0.14 \pm 0.02$. As in the synchrotron spectra, no signs of diffraction peaks of the $L6_0$ phase could be detected in the neutron spectra of this sample (Fig. 11). An assessment of its maximum possible volume fraction based on fluctuations in the background level suggests that it does not exceed 2%. This is ten times more than what follows from synchrotron

data, but noticeably less than in the previously mentioned references [16,19,24].

From the neutron diffraction patterns of the $Fe_{73}Ga_{27}$ alloy it clearly follows that in the as-cast state this alloy is in the $D0_3$ phase state. The microstructural state of the alloy is homogeneous, without any inclusions. This can be judged based on the Williamson-Hall construction for the widths of diffraction peaks. All experimental values of the full peak width at half maximum fall on a dependence whose parameters correspond to diffraction from homogeneous coherent scattering regions with a characteristic size of ≈ 1400 Å [41]. In the neutron patterns of this alloy, diffraction peaks of any other phases (including phase X) other than $D0_3$ were not detected.

IV. DISCUSSION

From the presented data it follows that in the studied $Fe_{81}Ga_{19}Tb_{0.1}$ and $Fe_{73}Ga_{27}$ alloys, none of the techniques we used showed the presence of the tetragonal $L6_0$ phase in the form of fairly extended domains (with characteristic sizes >50 Å) and a high level of atomic order. This fact is in clear contradiction with the results of many studies in which this phase was discovered using electron diffraction in both types of alloys. Three reasons can be formulated that could explain this contradiction.

(i) One of the most obvious is the assumption that electron diffraction is a much more sensitive method than photon or neutron diffraction and detects such a small volume fraction of the $L6_0$ phase that other techniques cannot detect. However, as was shown, the sensitivity level of the synchrotron (ID28) diffractometer on which the experiments were carried out allows one to reliably detect this phase if its fraction in the sample volume is $\delta(L6_0) \approx 0.2\%$ or more. Since it could not be registered, either its share is noticeably less than this level or it is absent from the sample. In this case, we have to admit that in Refs. [16,19,24], in which $\delta(L6_0)$ is

estimated in the range (3–5) %, they were mistaken in this estimate by about 20-fold, which is unlikely. In addition, if the volume fraction of the $L6_0$ phase is so small ($<0.2\%$), then it is unlikely that it could so effectively influence such a volumetric property of the alloy as magnetostriction. Indeed, according to the calculations given in Ref. [24], the level of magnetostriction observed in Fe-Ga alloys can be achieved if the volume fraction of the $L6_0$ phase is at least 4%.

(ii) It can be assumed that in TEM experiments some other phase is taken as $L6_0$. From the analysis of the structure factors of the $D0_3$ phase, it follows that any nonstandard ordering of the Fe and Ga atoms within its structure leads to the appearance of diffraction peaks that are forbidden in $D0_3$. For example, the $Fe_{81}Ga_{19}$ alloy can be represented with a good approximation as $Fe_{13}Ga_3$ with one "extra" Fe atom in relation to the stoichiometric composition of $Fe_{12}Ga_4$. If this Fe atom statistically replaces Ga atoms in positions (8c), then the extinction rules for the $D0_3$ structure are preserved. If this atom is ordered in one of the (8c) positions, then diffraction peaks with any set of Miller indices become allowed, including peaks allowed in the $L6_0$ phase, such as 100, 101, etc. In this case, the structure factors of all superstructure peaks become about 1.5 times smaller than for $Fe_{75}Ga_{25}$, but this decrease is not critical for their detection.

(iii) Another possible assumption is the difference in sample preparation procedures for different experimental techniques. In the Introduction, it was noted that although the $L6_0$ phase is not equilibrium in Fe-Ga alloys, its formation can be caused by composition fluctuations, features of growth kinetics and specific heat treatment of the alloy. Accordingly, some seemingly insignificant details of sample preparation can significantly affect the total amount of this phase and its distribution in the sample volume. There are a number of studies in which x-ray (synchrotron) and TEM experiments were carried out in parallel, but superstructure diffraction peaks of the $L6_0$ phase were observed only by the SAED technique, and only splitting of the fundamental peaks was recorded in the x-ray (synchrotron) patterns (e.g., Refs. [16,18]), which was taken to be tetragonal. However, as shown above, the interpretation of the position and intensities of the components raises a number of questions and cannot serve as a reliable indicator of the presence of the $L6_0$ phase.

In our opinion, the most plausible explanation for this contradiction may be the last assumption about the radical influence of different sample preparations for synchrotron-neutron and TEM experiments on the results obtained. In the case of diffraction of synchrotron or neutron radiation, the influence of sample preparation for the experiment can be considered insignificant and, accordingly, does not affect the results obtained. The observed differences in the results obtained by these two methods are determined only by the specifics of the interaction of the corresponding radiation with matter. For example, in neutron studies of alloys, splitting of the fundamental peaks has never been observed. On the contrary, this splitting is regularly seen in x-ray and synchrotron experiments. As shown in Ref. [27], this feature is fully explained by the different penetration depths of these radiations.

It is known that sample preparation for a TEM experiment is very specific; in particular, this procedure involves a sig-

nificant impact on the sample, during which the formation of nonstandard structural phases is possible. Our TEM studies used the method of two-jet electrochemical polishing of disks before their perforation in a 5% solution of perchloric acid in methanol, at a temperature of $-30\,°C$. In samples prepared using this method, the $L6_0$ phase is not observed (see Sec. III B). Basically, to prepare samples for TEM experiments, the focused ion-milling beam (FIB) technique is used (see, for example, Refs. [18,23,24]), which often leads to the appearance of precipitates on the surface of the samples in the form of iron oxides, and possibly also the $L6_0$ phase. Another possible consequence of preparing a sample by the FIB technique is the ordering of Fe in one of the (8c) positions and, as a consequence, the appearance of diffraction peaks simulating the $L6_0$ phase.

V. CONCLUSIONS

From complementary analysis of detailed electron, synchrotron, and neutron diffraction data obtained for the $Fe_{81}Ga_{19}Tb_{0.1}$ and $Fe_{73}Ga_{27}$ alloys, it follows that their average structures ($A2$ and $D0_3$, respectively) are consistent with expectations based on already published papers. Additional types of ordering are $D0_3$ clusters with $L_{coh} \approx 300\,Å$ in $Fe_{81}Ga_{19}Tb_{0.1}$ and the hexagonal or orthorhombic X phase in $Fe_{73}Ga_{27}$. None of the methods used showed the presence of tetragonal phases $L6_0$ and $D0_{22}$ observed in Ref. [14]. Tetragonal splitting of the fundamental diffraction peaks, which could indicate the presence of these phases in the sample, was also not observed. Analysis of the level of background fluctuations in the locations of superstructure peaks of the $L6_0$ phase made it possible to obtain an upper estimate for the volume fraction of this phase in the sample. Namely, assuming a stoichiometric composition ($Fe_{75}Ga_{25}$) and a maximum level of ordering ($\xi = 1$), it was found that its volume fraction does not exceed 0.2%.

For the composition $Fe_{73}Ga_{27}$, close to stoichiometric Fe_3Ga, reliable data were obtained using the SAED method and an ID28 diffractometer (ESRF) confirming the presence of phase X in the crystal, indications of the existence of which were first presented in Ref. [29]. Reflections of this phase can be indexed in a cubic lattice with a parameter $a = 3a(D0_3) \approx 17.34\,Å$, and can simulate a primitive cubic group with $a = a(D0_3)$, including reflections from the $L6_0$ phase if it would be present in the sample. The fraction of this phase in the sample volume hardly exceeds 0.1%.

Several hypotheses have been proposed that could explain the contradiction of the listed facts with data published in a number of articles on the existence of the $L6_0$ tetragonal phase with a volume fraction at the level of 3–5 % in Fe-Ga alloys with a Ga content of 17–27 at. %. A likely explanation for this situation is the assumption that differences in sample preparation for synchrotron-neutron and TEM experiments have a radical influence on the results obtained. Another option may be the assumption that in bulk samples the $L6_0$ phase does not form regions with long-range order, but exists only in the form of LCO domains with a tetragonal $L6_0$-type structure [13] with a very short coherence length.

Starting from Refs. [4,5], the answer to the question about the physical reasons for the increased magnetostriction of

Fe-Ga alloys was sought among the factors causing tetragonal distortions of the initially cubic atomic structure of the alloy. Calculations performed in Refs. [6,42,43] demonstrated that Ga-Ga pairs, representing element B2 of the structure, are the minimum defect leading to increased magnetostriction of Fe-Ga alloys. Experimental evidence of the formation of "*B*2 clusters" in a cubic matrix and its accompanying tetragonal distortion is the observation of diffuse scattering of neutron [10] and x-ray [12] radiation in Fe-Ga single crystals. Confirmation of the possibility of increasing the magnetostriction constant during the formation of "*B*2 clusters" is indirectly contained in the results of Ref. [44], in which systematic density functional theory calculations were carried out for cells containing two pairs of ordered Ga atoms, simulating the $L6_0$ structure. Leaving one pair of ordered Ga atoms in the cells, the transition to the *B*2 cluster may affect the magnitude of the effect of increasing the magnetostriction constant, but is unlikely to eliminate it completely. It should be noted that *B*2 clusters are also present in other types of Fe-based alloys, for example, in Fe-Si [45] and Fe-Al [46].

In this regard, the results obtained using extended x-ray absorption fine structure [47] and differential x-ray absorption spectroscopy [48] methods for $Fe_{80}Ga_{20}$ and $Fe_{81}Ga_{19}$, respectively, are important. Particularly indicative are the data on perturbations of the local atomic structure presented in Ref. [48], from which it follows that the shifts of Fe atoms surrounding the Ga-Ga pair are sufficient for the observed increase in the magnetostriction constant. In this model it is assumed that Ga-Ga pairs are randomly arranged throughout the material and the required effect is achieved without the organization of short- or long-range order with the structure of $L6_0$ type.

[1] A. E. Clark, J. B. Restorff, M. Wun-Fogle, T. A. Lograsso, and D. L. Schlagel, Magnetostrictive properties of body-centered cubic Fe-Ga and Fe-Ga-Al alloys, IEEE Trans. Magn. **36**, 3238 (2000).

[2] A. E. Clark, K. B. Hathaway, M. Wun-Fogle, J. B. Restorff, T. A. Lograsso, V. M. Keppens, G. Petculescu, and R. A. Taylor, Extraordinary magnetoelasticity and lattice softening in bcc Fe-Ga alloys, J. Appl. Phys. **93**, 8621 (2003).

[3] E. M. Summers, T. A. Lograsso, and M. Wun-Fogle, Magnetostriction of binary and ternary Fe–Ga alloys, Mater. Sci. **42**, 9582 (2007).

[4] A. E. Clark, M. Wun-Fogle, J. B. Restorff, T. A. Lograsso, and J. R. Cullen, Effect of quenching on the magnetostriction of $Fe_{1-x}Ga_x$ (0.13 < x < 0.21), IEEE Trans. Magn. **37**, 2678 (2001).

[5] J. R. Cullen, A. E. Clark, M. Wun-Fogle, J. B. Restorff, and T. A. Lograsso, Magnetoelasticity of Fe–Ga and Fe–Al alloys, J. Magn. Magn. Mater. **226-230**, 948 (2001).

[6] R. Wu, Origin of large magnetostriction in FeGa alloys, J. Appl. Phys. **91**, 7358 (2002).

[7] T. A. Lograsso, A. R. Ross, D. L. Schlagel, A. E. Clark, and M. Wun-Fogle, Structural transformation in quenched Fe-Ga alloys, J. Alloys Compd. **350**, 95 (2003).

[8] G. Khachaturyan and D. Viehland, Structurally heterogeneous model of extrinsic magnetostriction for Fe-Ga and similar magnetic alloys: Part I. Decomposition and confined displacive transformation, Metall. Mater. Trans. A **38**, 2308 (2007).

[9] S. Bhattacharyya, J. R. Jinschek, A. Khachaturyan, H. Cao, J. F. Li, and D. Viehland, Nanodispersed DO_3-phase nanostructures observed in magnetostrictive Fe–19% Ga Galfenol alloys, Phys. Rev. B **77**, 104107 (2008).

[10] H. Cao, P. M. Gehring, C. P. Devreugd, J. A. Rodriguez-Rivera, J. Li, and D. Viehland, Role of nanoscale precipitates on the enhanced magnetostriction of heat-treated galfenol ($Fe_{1-x}Ga_x$) alloys, Phys. Rev. Lett. **102**, 127201 (2009).

[11] H. Cao, P. M. Gehring, C. P. Devreugd, J. A. Rodriguez-Rivera, J. Li, and D. Viehland, Erratum: Role of nanoscale precipitates on the enhanced magnetostriction of heat-treated galfenol ($Fe_{1-x}Ga_x$) alloys, Phys. Rev. Lett. **105**, 119904(E) (2010).

[12] Yu. P. Chernenkov, N. V. Ershov, and V. A. Lukshina, Effect of annealing in a ferromagnetic state on the structure of an Fe–18 at % Ga alloy, Phys. Solid State **60**, 2370 (2018).

[13] K. Yan, Y. Xu, J. Niu, Y. Wu, Y. Li, B. Gault, S. Zhao, X. Wang, Y. Li, J. Wang, K. P. Skokov, O. Gutfleisch, H. Wu, D. Jiang, Y. He, and C. Jiang, Unraveling the origin of local chemical ordering in Fe-based solid-solutions, Acta Mater. **264**, 119583 (2024).

[14] J. Gou, T. Yang, R. Qiao, Y. Liu, and T. Ma, Formation mechanism of tetragonal nanoprecipitates in Fe–Ga alloys that dominate the material's large magnetostriction, Scr. Mater. **185**, 129 (2020).

[15] Y. Ke, C. Jiang, J. Tao, and H. Duan, Local inhomogeneous structural origin of giant magnetostriction in Fe-Ga alloys, J. Alloys Compd. **725**, 14 (2017).

[16] Y. He, X. Ke, C. Jiang, N. Miao, H. Wang, J. M. D. Coey, Y. Wang, and H. Xu, Interaction of trace rare earth dopants and nanoheterogeneities induces giant magnetostriction in Fe-Ga alloys, Adv. Funct. Mater. **28**, 1800858 (2018).

[17] Y. Han, H. Wang, T. Zhang, Y. He, and C. Jiang, Exploring structural origin of the enhanced magnetostriction in Tb-doped $Fe_{83}Ga_{17}$ ribbons: Tuning Tb solubility, Scr. Mater. **150**, 101 (2018).

[18] T. Jin, H. Wang, Y. Chen, T. Li, J. Wang, and C. Jiang, Evolution of nanoheterogeneities and correlative influence on magnetostriction in FeGa-based magnetostrictive alloys, Mater. Charact. **186**, 111780 (2022).

[19] B. Chen, Y. Gong, Z. Zhang, Z. Lu, S. Pan, Y. Guo, and F. Xu, Microstructure related disparity of the magnetostriction in the ⟨100⟩ oriented directionally solidified $Fe_{81}Ga_{19}$ polycrystals, Scr. Mater. **227**, 115296 (2023).

[20] C. Mudivarthi, M. Laver, J. Cullen, A. Flatau, and M. Wuttig, Origin of magnetostriction in Fe-Ga, J. Appl. Phys. **107**, 09A957 (2010).

[21] M. Laver, C. Mudivarthi, J. R. Cullen, A. B. Flatau, W.-C. Chen, S. M. Watson, and M. Wuttig, Magnetostriction and magnetic heterogeneities in iron-gallium, Phys. Rev. Lett. **105**, 027202 (2010).

[22] J. Gou, T. Ma, X. Liu, C. Zhang, L. Sun, G. Sun, W. Xia, and X. Ren, Large and sensitive magnetostriction in ferromagnetic composites with nanodispersive precipitates, NPG Asia Mater. **13**, 6 (2021).

[23] C. Zhang, J. Gou, J. Yang, T. Ma, L. Sun, G. Sun, Q. Tian, G. Yan, L. Chen, P. Zhang, and Y. Liu, Nanoheterogeneity response in large-magnetostriction Fe-Ga alloys: An in-situ magnetic small-angle neutron scattering study, Acta Mater. **225**, 117594 (2022).

[24] Y. Wu, Y. Chen, Ch. Meng, H. Wang, X. Ke, J. Wang, J. Liu, T. Zhang, R. Yu, J. M. D. Coey, Ch. Jiang, and H. Xu, Multiscale influence of trace Tb addition on the magnetostriction and ductility of ⟨100⟩ oriented directionally solidified Fe-Ga crystals, Phys. Rev. Mater. **3**, 033401 (2019).

[25] H. Liu, Y. Wang, L. Dong, H. Wang, Y. Zhang, Z. Zhang, and W. Tan, Structure and magnetic properties of Fe–Ga ribbons doped by Sn, J. Mater. Sci.: Mater. Electron. **32**, 745 (2021).

[26] Z. Dai, C. Zhou, C. Guo, K. Cao, R. Zhang, T. Chang, Y. Matsushita, A. Murtaza, F. Tian, W. Zuo, Y. Zhang, S. Yang, and X. Song, Giant enhancement of magnetostriction in Pt doped FeGa ribbons, Appl. Phys. Lett. **123**, 082402 (2023).

[27] S. V. Sumnikov, I. A. Bobrikov, I. S. Golovin, and A. M. Balagurov, Bulk vs. surface structural phases in Fe-27Ga alloy, J. Alloys Compd. **928**, 167116 (2022).

[28] Yu. P. Chernenkov, N. V. Ershov, and V. A. Lukshina, Finding a new *B*1-type phase in single crystals of Fe–Al and Fe–Ga soft magnetic alloys, Phys. Solid State **61**, 1960 (2019).

[29] A. M. Balagurov, D. Yu. Chernyshov, A. A. Bosak, I. A. Bobrikov, S. V. Sumnikov, and I. S. Golovin, In-grain phase separation and structural ordering in Fe-Ga alloys seen from reciprocal space, Intermetallics **128**, 107016 (2021).

[30] J. B. Restorff, M. Wun-Fogle, K. B. Hathaway, A. E. Clark, T. A. Lograsso, and G. Petculescu, Tetragonal magnetostriction and magnetoelastic coupling in Fe-Al, Fe-Ga, Fe-Ge, Fe-Si, Fe-Ga-Al, and Fe-Ga-Ge alloys, J. Appl. Phys. **111**, 023905 (2012).

[31] V. Dyadkin, P. Pattison, V. Dmitriev, and D. Chernyshov, A new multipurpose diffractometer PILATUS@SNBL, J. Synchrotron Rad. **23**, 825 (2016).

[32] A. Girard, T. Nguyen-Thanh, S. M. Souliou, M. Stekiel, W. Morgenroth, L. Paolasini, A. Minelli, D. Gambetti, B. Winkler, and A. Bosak, A new diffractometer for diffuse scattering studies on the ID28 beamline at the ESRF, J. Synchrotron Rad. **26**, 272 (2019).

[33] A. M. Balagurov, High resolution Fourier diffraction at the IBR-2 reactor, Neutron News **16**, 8 (2005).

[34] A. M. Balagurov and I. S. Golovin, Neutron scattering in studies of Fe-based functional alloys (Fe-Ga, Fe-Al), Phys. Usp. **64**, 702 (2021).

[35] R. W. G. Wyckoff, *Crystal Structures* (John Wiley & Sons, New York, 1963).

[36] See Supplemental Material at http://link.aps.org/supplemental/ 10.1103/PhysRevMaterials.8.073604 for figures (eight in total) that illustrate statements made in the main text. They include model-calculated and experimentally measured profiles of neutron and synchrotron diffraction patterns, showing the absence of peaks from the $L6_0$ phase. In addition, they include TEM drawings confirming the presence of the X phase in the $Fe_{73}Ga_{27}$ sample.

[37] T. A. Lograsso and E. M. Summers, Detection and quantification of chemical order in Fe–Ga alloys using high resolution x-ray diffraction, Mater. Sci. Eng. A **416**, 240 (2006).

[38] I. S. Golovin, A. M. Balagurov, V. V. Palacheva, A. Emdadi, I. A. Bobrikov, A. Yu. Churyumov, V. V. Cheverikin, A. V. Pozdniakov, A. V. Mikhaylovskaya, and S. A. Golovin, Influence of Tb on structure and properties of Fe-19%Ga and Fe-27%Ga alloys, J. Alloys Compd. **707**, 51 (2017).

[39] I. S. Golovin, A. M. Balagurov, W. C. Cheng, J. Cifre, D. A. Burdin, I. A. Bobrikov, V. V. Palacheva, N. Yu. Samoylova, and E. N. Zanaeva, *In situ* studies of atomic ordering in Fe-19Ga type alloys, Intermetallics **105**, 6 (2019).

[40] A. M. Balagurov, I. S. Golovin, I. A. Bobrikov, V. V. Palacheva, S. V. Sumnikov, and V. B. Zlokazov, Comparative study of structural phase transitions in bulk and powdered Fe-27Ga alloy by real-time neutron thermodiffractometry, J. Appl. Cryst. **50**, 198 (2017).

[41] I. S. Golovin, A. K. Mohamed, V. V. Palacheva, V. V. Cheverikin, A. V. Pozdnyakov, V. V. Korovushkin, A. M. Balagurov, I. A. Bobrikov, N. Fazel, M. Mouas, J. -G. Gasser, F. Gasser, P. Tabary, Q. Lan, A. Kovacs, S. Ostendorp, R. Hubek, S. Divinski, and G. Wilde, Comparative study of structure and phase transitions in Fe-(25-27)%Ga alloys, J. Alloys Compd. **811**, 152030 (2019).

[42] J. Cullen, P. Zhao, and M. Wuttig, Anisotropy of crystalline ferromagnets with defects, J. Appl. Phys. **101**, 123922 (2007).

[43] M. V. Petrik, O. I. Gorbatov, and Yu. N. Gornostyrev, Role of magnetism in the formation of a short-range order in an Fe-Ga alloy, JETP Lett. **98**, 809 (2014).

[44] J. Niu, K. Yan, Y. Xu, Y. Wu, E. Liu, Z. Fu, J. Li, X. Gao, X. Mu, B. Liu, X. Wang, Y. Li, J. Wang, and C. Jiang, Understanding the intrinsic mechanism of the giant magnetostriction in binary and alloyed FeGa solid solutions, Phys. Rev. B **109**, 014417 (2024).

[45] Yu. P. Chernenkov, N. V. Ershov, V. A. Lukshina, V. I. Fedorov, and B. K. Sokolov, An x-ray diffraction study of the shortrange ordering in the soft-magnetic Fe–Si alloys with induced magnetic anisotropy, Phys. B: Condens. Matter. **396**, 220 (2007).

[46] N. V. Ershov, N. M. Kleinerman, V. A. Lukshina, Yu. P. Chernenkov, D. A. Shishkin2, O. P. Smirnov, and V. G. Semenov, Short-range order in "disordered" aluminum solid solutions in α-iron, Phys. Solid State **65**, 366 (2023).

[47] S. Pascarelli, M. P. Ruffoni, R. Sato Turtelli, F. Kubel, and R. Grössinger, Local structure in magnetostrictive melt-spun $Fe_{80}Ga_{20}$ alloys, Phys. Rev. B **77**, 184406 (2008).

[48] M. P. Ruffoni, S. Pascarelli, R. Grössinger, R. S. Turtelli, C. Bormio-Nunes, and R. F. Pettifer, Direct measurement of intrinsic atomic scale magnetostriction, Phys. Rev. Lett. **101**, 147202 (2008).